The International Journal of Robotics Research OnlineFirst, published on May 20, 2009 as doi:10.1177/0278364909101795

The RAVEN: Design and Validation of a Telesurgery System

Mitchell J. H. Lum
Diana C. W. Friedman
Ganesh Sankaranarayanan
Hawkeye King
Kenneth Fodero II
Rainer Leuschke
Blake Hannaford

Department of Electrical Engineering,
BioRobotics Lab
University of Washington,
Seattle, WA 98195, USA
{mitchlum, dwarden, rosen, ganeshs, hawkeye1, kfodero, rainer, blake}@u.washington.edu

Jacob Rosen

Department of Computer Engineering
Baskin School of Engineering
University of California
Santa Cruz, CA 95064, USA
rosen@ucsc.edu

Mika N. Sinanan

Department of Surgery,
Center for Video Endoscopic Surgery,
University of Washington,
Seattle, WA 98195, USA
mssurg@u.washington.edu

Abstract

The collaborative effort between fundamental science, engineering and medicine provides physicians with improved tools and techniques for delivering effective health care. Minimally invasive surgery (MIS) techniques have revolutionized the way a number of surgical procedures are performed. Recent advances in surgical robotics are once again revolutionizing MIS interventions and open surgery. In an earlier research endeavor, 30 surgeons performed 7 different MIS tasks using the Blue Dragon system to collect measurements of position, force, and torque on a porcine model. This data served as the foundation for a kinematic optimization of a spherical surgical robotic manipulator. Following the optimization, a seven-degree-of-freedom cable-actuated surgical manipulator was designed and integrated, providing all degrees of freedom present in manual MIS as well as wrist joints located at the surgical end-effector. The RAVEN surgical robot system has the ability to teleoperate utilizing a single bi-directional UDP socket via a remote master device. Preliminary telesurgery experiments were conducted using the RAVEN. The experiments illustrated the system's ability to operate in extreme conditions using a variety of network settings.

KEY WORDS—surgical robot, telesurgery, mobile robotic telesurgery, kinematic optimization, minimally invasive surgery, teleoperation, FLS, task performance, human machine interface, time delay, surgical stills

1. Introduction

Innovation in surgery allows surgeons to provide better health care to their patients. In particular, minimally invasive surgery

The International Journal of Robotics Research
Vol. 00, No. 00, Xxxxxxxx 2009, pp. 000–000
DOI: 10.1177/0278364909101795

Figures 1–4, 7, 10, 12, 14–17 appear in color online: http://ijr.sagepub.com

(MIS) reduces postoperative hospital stays to just over a day compared with more than a week when the procedure is performed "open" (Robinson and Stiegmann 2004). More precise, less invasive and inherently safer techniques and equipment are a natural part of the evolution of health care. In April 1985, Kwoh and colleagues used a Unimation Puma 200 robot to orient a biopsy needle for neurosurgery, marking the first use of robotics in surgery (Kwoh et al. 1988). The latter half of the 1980s also saw the development of the system that would later become ROBODOC, which was used for precision bone machining for orthopedic surgeries such as cementless total hip replacements first in canines and then in humans (Taylor et al. 1989, 1994), as well as the use of a robot to perform a transurethral resection of the prostate, first with a Unimate Puma 560 and later with the specially designed Probot (Davies et al. 1989; Davies 2000; Harris et al. 1997). The use of robotics in surgery increased in popularity in the 1990s, with devices such as the SRI telepresence system (Hill et al. 1994), the IBM Research Center/Johns Hopkins University surgical robot (Taylor et al. 1995), the system designed at the Politecnico di Milano in Italy (Rovetta et al. 1996), and the Black Falcon from Massachusetts Institute of Technology (Madhani et al. 1998).

The Automated Endoscopic System for Optimal Positioning (AESOP) was the first robot approved for use in surgery by the US Food and Drug Administration (FDA). After its approval in 1994, the system assisted surgeons by supporting an endoscope and repositioning according to the surgeons' instructions (Jacobs 1997; Sackier et al. 1997). Licensed by Computer Motion, Inc. (Goleta, CA), the AESOP was later incorporated into the Zeus robotic surgery system (Ghodoussi et al. 2002), which received FDA approval in October 2001. The Zeus was used in the first transatlantic telesurgery, performed between Manhattan, New York, USA and Strasbourg, France (Marescaux et al. 2001; Ghodoussi et al. 2002). The Zeus's major competitor was the da Vinci surgical robot, produced by Intuitive Surgical, Inc. (Mountain View, CA) and FDA approved in July 2000 (Guthart and Salisbury 2000). In June 2003, the companies merged under the name Intuitive Surgical, Inc. and production of the Zeus and AESOP systems ceased (Sim et al. 2006). Other commercially available systems include the NeuroMate (which, along with ROBODOC, was produced by Integrated Surgical Systems, Inc. in Davis, CA, until 2005) (Lavallèe et al. 1992; Cleary and Nguyen 2001) and the Naviot laparoscope manipulator (Hitachi Co., Japan) (Kobayashi et al. 1999).

Several surgical robotic systems are currently in development around the world. The system designed at the University of Tokyo (Mitsuishi et al. 2003) has performed telesurgical experiments throughout Asia. The NeuRobot (Hongo et al. 2002) has been used in clinical applications. Other systems include the Berkeley/UCSF laparoscopic telesurgical workstation (Cavusoglu et al. 2003), the Light Endoscopic Robot (Berkelman et al. 2003), and the MC^2E (Zemiti et al. 2007).

The University of Washington's RAVEN differs from previous systems because the design originated from a long-standing relationship with surgeons. The collaborative effort spawned an engineering approach, applied to surgery resulting in *in-vivo* measurements that quantified the tool–tissue interactions. The RAVEN manipulator is optimized based on this surgical data and validation studies using the Society of American Gastrointestinal Endoscopic Surgeons (SAGES) Fundamentals of Laparoscopic Surgery (FLS) skills tasks give results that are meaningful in the surgical context. This paper will discuss the design, development, and accomplishments of the RAVEN Surgical Robot.

2. Clinical Requirements

For over a decade and a half, strong collaboration between engineers in the BioRobotics Lab and surgeons in the Center for Video Endoscopic Surgery has focused on answering clinically relevant problems. Surgical training followed the mentor/student model whereby the expert surgeon shows a novice how to perform a task and the novice then mimics the expert. The evaluation of surgical skill has historically been a subjective process.

In order to move toward more objective measures, extensive work has been performed in the area of surgical measurement and skill assessment Rosen et al. (2006). The Blue Dragon, a passive device instrumented with sensors, was developed for measuring surgical tool displacements, forces and torques during *in vivo* animal surgeries (Figure 1). Using the Blue Dragon, an extensive database was created of *in-vivo* tissue handling/examination, dissection and suturing tasks performed by 30 surgeons. Analysis of this data indicated that 95% of the time the surgical tools were located within a conical range of motion with a vertex angle 60° (termed the dexterous workspace (DWS)). A measurement taken on a human patient showed that in order to reach the full extent of the abdomen, the tool needed to move 90° in the mediolateral (left to right) and 60° in the superior/inferior direction (head to foot). The extended dexterous workspace (EDWS) was defined as a conical range of motion with a vertex angle of 90° and is the workspace required to reach the full extent of the human abdomen without reorientation of the base of the robot. These parameters, obtained through surgical measurement, served as a basis for the kinematic optimization of the RAVEN spherical mechanism.

3. Robot Design

The RAVEN Surgical Robot consists of three main pieces: the patient site, the surgeon site and a network connecting the two. Using the typical teleoperator system nomenclature the surgeon site is the "master" and the patient site is the "slave".

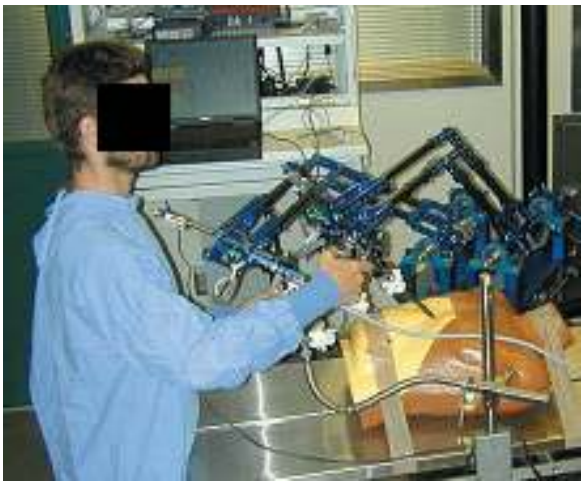

(a)

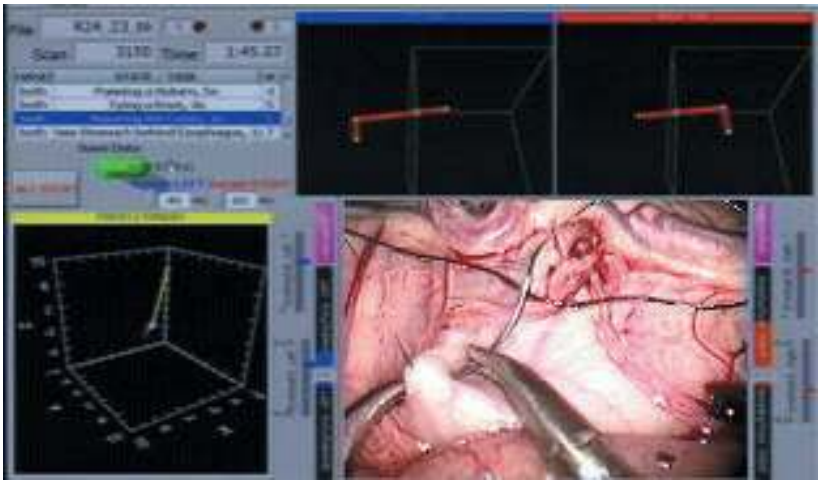

(b)

Fig. 1. The Blue Dragon system. (a) The system integrated into a MIS operating room. (b) Graphical user interface showing the position and orientation of each tool with respect to the port as well as an overlaid video feed from the endoscope.

The patient site consists of two surgical manipulators that are positioned over the patient. The surgeon site consists of two control devices and a video feed from the operative site. The communication layer can be any TCP/IP network including a local private network, the Internet or even a wireless network.

3.1. The Patient Site

Much of the engineering effort was focused on developing the patient site. Starting with the range of motion required for surgery, the spherical mechanism was analyzed and optimized for this application (Lum et al. 2006). The optimization determined the most compact mechanism with the best kinematic performance in the workspace required for surgery. Once the optimal geometry of the mechanism was determined, a detailed design of the arms and tool interface was performed to yield a lightweight and rigid pair of manipulators.

3.1.1. Design Approach

The pivot point constraint in MIS makes the spherical manipulator a natural candidate for a surgical robot. The CMI Zeus system used a SCARA-like manipulator and required a MIS port to constrain its motion. A spherical mechanism inherently allows rotation about a remote center requiring neither a physical constraint nor a complex controller to prevent tangential motion or forces about the incision. The spherical mechanism allows the robot to be operated under both MIS and "open"

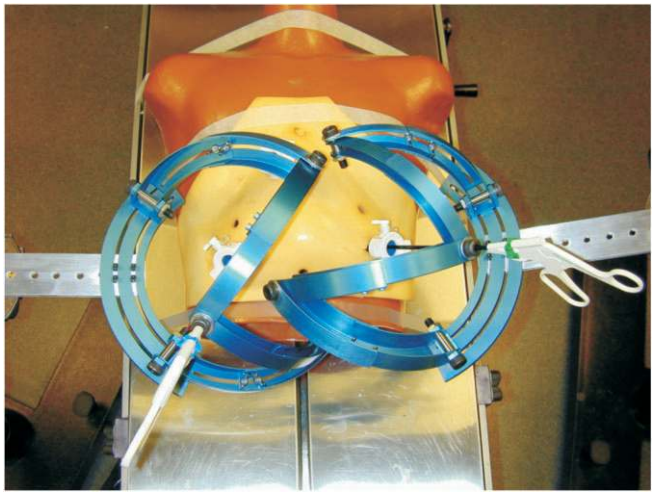

Fig. 2. Two parallel mechanism aluminum mock-ups. The parallel mechanism has four links and would have two actuated joints (the two base joints) if used for a surgical robot. It is clear from this figure that the parallel mechanism suffers from collision problems. The dry-lab experiments underscored the need for the most compact mechanism possible.

surgery configurations with no change to the system whatsoever.

An adjustable passive aluminum mock-up was fabricated to model the kinematics of the spherical manipulator in parallel and serial configurations. The link angles of the spherical mechanism are the angles between adjacent revolute joints. The base angle is the angle between the two most proximal revolute joints of the parallel manipulator, which would be the two actuated joints for the robotic mechanism. The mock-up was designed such that a standard MIS tool with 5 mm shaft could pass through the distal joint. In a dry-lab set-up, a number of kinematic configurations were compared on a training torso (Simulab, Seattle, WA) to assess the range of motion and collision problems. These dry-lab experiments showed that a parallel configuration had a limited workspace with kinematic singularities contained in the workspace, self-collision problems (where an arm collided with itself), robot–robot collisions (between two robots within the surgical scene) and robot–patient collisions (Figure 2). Based on some of these practical constraints it was determined that the best configuration was two serial manipulators.

The wet-lab experiment applied results from the dry-lab experiment; two serial manipulators were evaluated with surgeons performing suturing and tissue-handling tasks *in vivo* on a porcine model as shown in Figure 3. For this evaluation the link angles were set to 75° and the surgeons were able to perform all of the required tasks without robot–robot or robot–patient collisions. The wet-lab experiment validated that two serial spherical manipulators in the surgical scene would be feasible for a surgical robotic system.

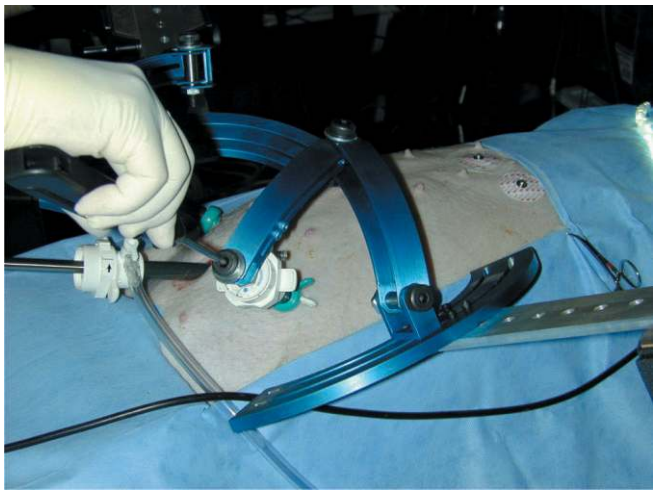

(a)

(b)

Fig. 3. (a) Close-up photo of two serial mechanisms in the wet-lab set-up. (b) Surgeons manipulating conventional tools inserted through the last axis of the mock-ups using the serial configuration.

The detailed numerical analysis of Lum (2004) analyzed both the parallel and serial mechanism and confirmed the results of the experimental evaluation. A kinematic optimization was performed to determine the optimal link angles based on the workspace required for surgery. One striking result is that for base angles greater than zero (both joint axes collinear), the parallel mechanism is plagued by an area of kinematic singularity within the center of its workspace (Figure 4).

It was shown both experimentally and analytically that the serial mechanism is better suited as a surgical manipulator. In this study, optimization criteria consisted of kinematic isotropy (the ratio of singular values of the Jacobian matrix) in the numerator and a link length penalty in the de-

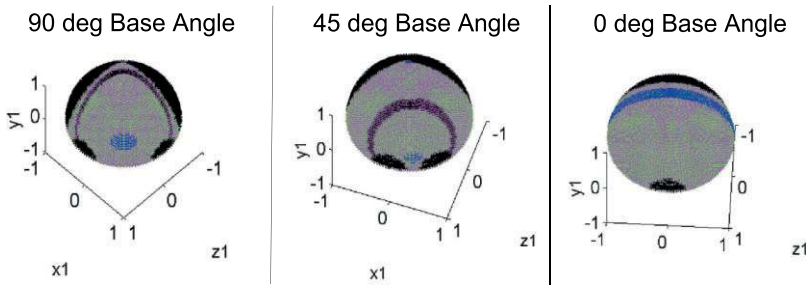

Fig. 4. The workspace is shown for the parallel mechanism with four equal link lengths of 60° as a function of three different base angles $\alpha_{12} = 90°, 45°, 0°$. Black represents areas outside the reachable workspace or areas near kinematic singularity. The circular area in the center of the workspace for the 90° and 45° bases and the stripe for the 0° base represent and area of greatest isotropy. Note that for the 90° and 45° bases and area of singularity cuts through the reachable workspace, a property that is highly undesirable.

nominator. The combined criterion rewards good kinematic performance and penalizes size. With this criterion at its core, the optimization was performed comprehensively over the design space with all combinations of each link ranging from 30° to 90°. Within each design candidate the target workspace was the DWS, the 60° cones. Only the designs that could also reach the EDWS were considered. The optimization resulted in a design of 75° for the first link angle and 60° for the second link angle. The optimized link angles served as the foundation for extensive mechanical design.

3.1.2. Surgical Manipulators

The seven-degree-of-freedom (7-DOF) cable-actuated surgical manipulator, shown in Figure 5, is broken into three main pieces: the static base that holds all of the motors; the spherical mechanism that positions the tool; and the tool interface. The motion axes of the surgical robot are:

1. the shoulder joint (rotational);
2. the elbow joint (rotational);
3. tool insertion/retraction (translational);
4. tool rotation (rotational);
5. tool grasping (rotational);
6. tool wrist-1 actuation (rotational);
7. tool wrist-2 actuation (rotational).

The first four joint axes intersect at the surgical port location, creating a spherical mechanism that allows for tool manipulation similar to manual laparoscopy. The mechanism links are machined from aluminum, and are generally I-section

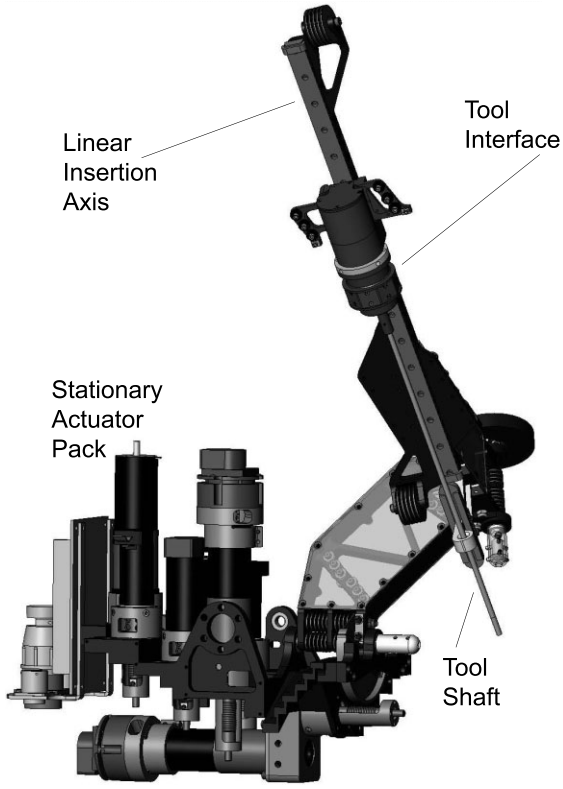

Fig. 5. CAD rendering of surgical manipulator shown with plastic covers removed. Mass: 12.3 kg; folded dimensions 61 cm × 53 cm × 38 cm; extended dimensions: 120 cm × 30 cm × 38 cm.

shapes with structural covers. These removable covers allow access to the cable system, while improving the torsional stiffness of the links. The links are also offset from the joint axis planes, allowing for a tighter minimum closing angle of the elbow joint.

The RAVEN utilizes DC brushless motors located on the stationary base, which actuate all motion axes. Maxon EC-40 motors with 12:1 planetary gearboxes are used for the first three axes, which see the highest forces. The first two axes, those under the greatest gravity load, have power-off brakes to prevent tool motion in the event of a power failure. The fourth axis uses an EC-40 without a gearbox, and Maxon EC-32 motors are used for the remaining axes. Maxon DES70/10 series amplifiers drive these brushless motors. The motors are mounted onto the base via quick-change plates that allow motors to be replaced without the need to disassemble the cable system.

The cable transmission system comprises a capstan on each motor, a pretension adjustment pulley, various pulleys to redirect the cables through the links, and a termination point to each motion axis. The shoulder axis is terminated on a single partial pulley. The elbow axis has a dual-capstan reduction stage terminating on a partial pulley. The tool insertion/retraction axis has direct terminations of the cables on the tool holder. The tool rotation, grasping, and wrist cables are terminated on capstans on the tool interface.

The cable system transmission ratios for positioning the tool tip are as follows.

1. Shoulder: 7.7:1 (motor rotations:joint rotations).
2. Elbow: 7.3:1 (motor rotations:joint rotations).
3. Insertion: 133:1 (radians:meters).

Each axis is controlled by two cables, one for motion in each direction, and these two cables are pretensioned against each other. The cables are terminated at each end to prevent any possibility of slipping. The cable system maintains constant pretension on the cables through the entire range of motion. Force and motion coupling between the axes is accommodated for in the control system.

Laser pointers attached to the shoulder and elbow joints allow for visual alignment of the manipulator relative to the surgical port. When the two dots converge at the port location, the manipulator is positioned such that its center of rotation is aligned with the pivot point on the abdominal wall. The power-off brakes can be released by flipping a switch located on the base. The brakes are normally powered by the control electronics, but also have a battery plug-in for easy set-up and breakdown when the system is not powered. ABS plastic covers were created on a three-dimensional printer to encapsulate the motor pack thereby protecting actuators, encoders and electrical wiring. Figure 7(a) shows the complete patient site.

The tool interface, shown in Figure 6, controls the tool rotation, grasp, and wrist axes, and allows for quick changing of tools. The coupler is designed for one-handed engagement/disengagement of the surgical tool to the manipulator. The tools used are Micro-Joint tools from the Zeus surgical robot that have been adapted for use on the RAVEN. The tools' grasp and wrist axes are actuated by pushrods in the tool shaft. High pitch acme threads in the tool interface convert the rotational motion of the cable system capstans into linear motion of the tool pushrods. As the modified Zeus tools only feature

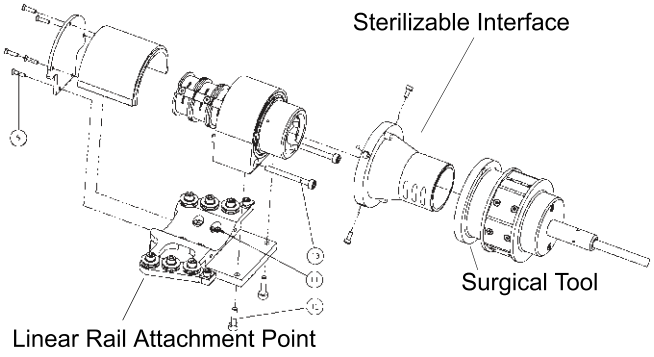

Fig. 6. Line drawing of the tool interface, exploded view.

(a)

(b)

Fig. 7. (a) The RAVEN patient site and (b) the surgeon site.

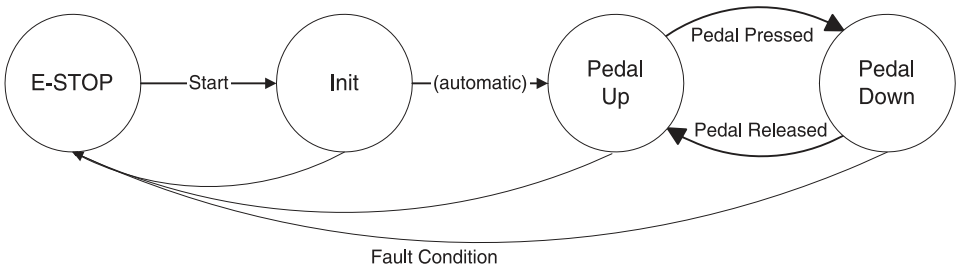

Fig. 8. Control system state diagram.

one wrist axis, the surgical robot currently utilizes one of its two wrist axes.

3.2. The Surgeon Site

The surgeon site was developed to be low cost and portable, a choice that allows for easier telesurgical collaboration. It consists of two PHANToM Omni devices (SensAble Technologies, Woburn, MA), a USB foot-pedal, a laptop running the surgeon's graphical user interface software, and a video feed of the operative site as shown in Figure 7(b). SensAble's PHANToM haptic devices are well established amongst haptics researchers with a development environment that is straightforward to use. The Omni is a cost effective solution that allowed us to quickly implement a surgeon interface device for our master/slave system. It features 3-DOF force-feedback, 6-DOF sensing and two momentary switches on the stylus. The RAVEN does not currently utilize the force-feedback capability of the Omni. The foot-pedal enables and disables the coupling between the patient site and surgeon site allowing for position indexing.

4. Software and Control

4.1. Patient Site

Control software is running in the kernel space of an RTAI Linux computer at a rate of 1 kHz. The critical link between the control software and the motor controllers is a USB 2.0 interface board. Our USB board features eight channels of high-resolution 16 bit D/A for control signal output to each controller and eight 24 bit quadrature encoder readers.

4.1.1. Software and Safety Architecture

The control system and surrounding electronic hardware were designed to incorporate safety, modular design, and flexibility. As this is a medical device, the most critical of these aspects is safety. Inherent to a safe system is robustness, reliability, and some level of automatic override. To achieve reliability we defined four software states in which our system can operate: initialization, pedal up, pedal down, and emergency stop (Figure 8). At power-up, the manipulators are resting against hard stops. The initialization state takes each manipulator from its resting position and moves it into the surgical field. Once the initialization is complete the system automatically transitions into the pedal up state. In the pedal up state the robot is not moving and brakes are engaged. The system enters pedal up when the surgeon lifts their foot from the foot pedal, decoupling the master from the surgical manipulator. This is done to perform tool indexing or free the surgeon's hands for peripheral tasks. The pedal down state is initiated when the surgeon pushes the foot pedal down, releasing the brakes and allowing the master device to directly control the surgical manipulator.

A Direct Logic 05 programmable logic controller (PLC) controls motor-enable, the brakes, and the system states based on inputs received from the system. PLCs are a robust technology used extensively in automation applications. PLC technology is reliable and provides built-in, easy-to-use safety circuitry. In addition to monitoring the system hardware, the PLC monitors the state of the control software through the use of a watchdog timer. The watchdog timer monitors a square-wave signal generated by the control software, output from the parallel port of the Linux PC. In the event of a software or computer hardware failure, the PLC will detect the loss of the square-wave and immediately put the system into the emergency stop state, enabling the brakes and disabling the motors. An array of status LEDs displays the current state of the system. The RTAI Linux control software detects state transitions of the PLC and follows them within 1 ms.

4.1.2. Gravity Compensation

Gravity introduces torques on the robot links that a control system has to combat to maintain a nominal pose, in addition to any environmental forces encountered by the end-effector. A model-less, closed-loop control system, such as PID, does not

take these gravitational effects into account. While a closed-loop controller can compensate to an extent for this disturbance effect, its ability to respond to movement commands is degraded by the additional load. By adding gravity compensation, the controller responds only to user input, and the system is more responsive. Only the first two joints of the RAVEN require compensation for gravity; the last four have enough friction that gravity does not significantly effect their dynamics.

The direct Lagrangian method was employed to calculate the expected gravity torque on each link (Checcacci et al. 2002). Potential energy of the RAVEN robot links can be given by

$$E_p = -m_1[{}^0g^T][{}^0_1R][{}^1c_1] - m_2[{}^0g^T][{}^0_2R][{}^2c_2] - m_3[{}^0g^T]({}^0l_3 + [{}^0_3R][{}^3c_3]),$$

where E_p is the potential energy of the system, m_n is the mass of link n, and ${}^nc_n$ is the center of mass of link n described in a coordinate frame attached to that link. The mass and center of mass values are taken from the CAD models of the system. Here ${}^0_nR$ is the rotation matrix describing the orientation of points in coordinate frame n, in coordinate frame zero. The rotation matrix is derived from the robot kinematics equations. The gravity vector, described in the base frame, is given by ${}^0g$. Finally, ${}^0l_3$ is the insertion displacement of the tool carriage, measured in the base frame.

The gravitational torque on a joint is the partial derivative of E_p with respect to that joint. The vector of gravity torques is then

$$G(\Theta) = \frac{\partial E_p}{\partial \Theta} = \begin{bmatrix} \frac{\partial E_p}{\partial \theta_1} \\ \frac{\partial E_p}{\partial \theta_2} \\ \frac{\partial E_p}{\partial d_3} \end{bmatrix},$$

where Θ is a vector of the joint variables, θ_1, θ_2, and d_3 (tool carriage insertion). Using the first two elements above, the expected gravitational torques on links one and two were added to the controller torque applied by the actuators. The RAVEN did not initially have gravity compensation, and the surgeons' response to this improvement has been overwhelmingly positive.

4.1.3. Engineers' Interface

The engineers' interface (EI), a low-level interface to the states and mechanisms of the control software, assists robot development. Developers are presented with an intuitive GUI with easy access to robot features. In development stages, the system run level (stop, init, run, e-stop) can be set manually with the click of a button. Control commands can be sent to any degree of freedom or the entire robot. For example, a 40° sine wave can be output on the shoulder joint, the motor controller number two can output 30% maximum current, or the end-effector position can be instructed to move 3 cm to the left. Furthermore, robot information (such as motor output, joint position, and end-effector position) is displayed on-screen in real-time, and also logged for later evaluation.

The EI can connect to the RTAI Linux control system using either FIFO device nodes or a single, bi-directional (TCP/IP) network socket. Two types of data are exchanged: a packet containing all robot-state information is received by the EI, and a command packet with all instruction parameters is sent from the EI to the control software. This link is independent of the master–slave link.

4.2. Surgeon Site

The surgeon site software provides the surgeon with a GUI to log-in and connect to the patient site. It allows for the unique identification of each user, keeping a detailed log of when each user logs into the system, connects to the patient site and transitions between pedal-up and pedal-down states. It provides an automatic means by which each user's time on the system can be tracked.

5. Experiments

The first teleoperation of the RAVEN took place on October 15, 2005 in a cross-campus demonstration at the University of Washington (UW) with the surgeon site in a lecture hall and the patient site in the BioRobotics Lab (BRL). The surgical manipulator's first three DOFs, the shoulder, elbow and tool insertion joints, were actuated. A PHANToM Omni was used to control the endpoint of the surgical tool through the UW's campus network with no noticeable delay.

The implementation of a low-cost and portable surgeon site has provided the opportunity for telesurgical collaboration. The telesurgery experiments summarized in Table 1 have included many topologies including within one lab, between labs, and mobile robotic telesurgery experiences. Figure 9 is a functional block diagram of the system, illustrating the key components of the patient site, the surgeon site, and the communication layer between them. The RAVEN has been tested in a variety of environments using a multiple communication layer topologies and has demonstrated its portability and robustness.

5.1. High Altitude Platforms/Mobile Robotic Telesurgery

Many research systems live out their entire life cycle in a laboratory environment, from conception to decommission, and

Table 1. Summary of Telesurgery Experiments

Experiment	Date(s)	Patient site	Surgeon site	Communication layer	
				Video	Network architecture
HAPs/MRT	June 5–9, 2006	Field, Simi Valley, CA	Field, Simi Valley, CA	HaiVision Hai560	Wireless via UAV
ICL	July 20, 2006	BioRobotics Lab, Seattle, WA	Imperial College, London, England	iChat or Skype	Commercial Internet
Animal Lab	March 8, 2007	CVES, Seattle, WA	CVES, Seattle, WA	Direct S-video	LAN
NEEMO Aquarius	May 8–9, 2007	Aquarius Undersea Habitat, 3.5 miles off Florida Keys, 60 ft depth	University of Washington, Seattle	HaiVision Hai1000	Commerical Internet between Seattle, WA and Key Largo, FL; microwave communication link across 10 miles, Key Largo to Aquarius
NEEMO NURC	May 12–13, 2007	National Undersea Research Center, Key Largo, FL	University of Washington, Seattle	HaiVision Hai200	Commercial internet

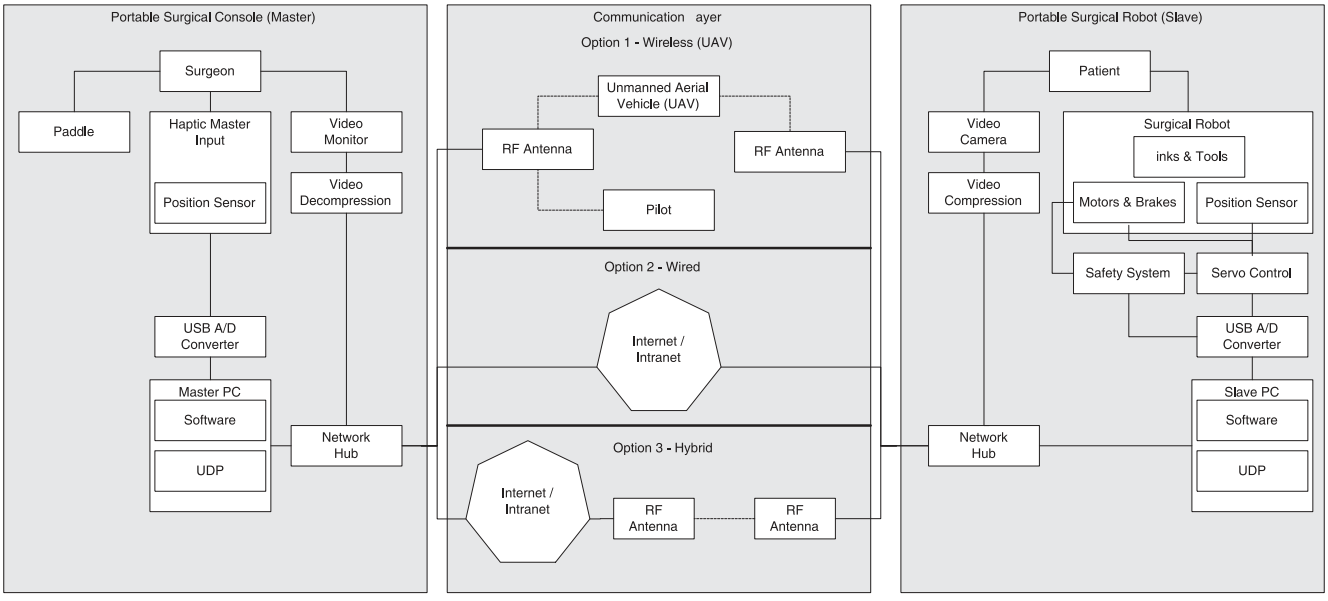

Fig. 9. RAVEN functional block diagram. The communication layer can take a few different forms including wireless UAV (HAPs/MRT), Wired (ICL, within lab experiments, animal lab), or hybrid (NEEMO) configurations.

are never challenged to move outside of that environment. A testament to the RAVEN's robustness was its first field deployment that took place June 5–9, 2006. Dr Timothy Broderick, Charles Doarn, and Brett Harnett of the University of Cincinnati led the High Altitude Platforms/Mobile Robotic Telesurgery (HAPs/MRT) project to evaluate surgical robotics in field conditions. As a collaborator in the HAPs/MRT project, the RAVEN was taken from the BRL in Seattle, WA, and deployed in the desert of Simi Valley, CA for telesurgery experiments on an inanimate model (see Figure 12). The system was powered by gas generators and was set up under portable tents in an isolated field. Separated by a distance of 100 m, the surgeon and patient sites were connected via an aerial digital datalink on-board AeroVironment's PUMA unmanned aircraft. The datalink provided by AeroVironment utilized Internet-style communication at a rate of 1 MB per sec-

(a)

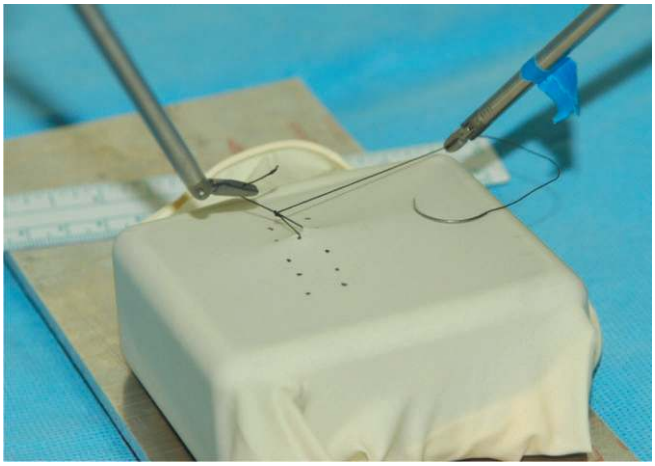

(b)

Fig. 10. (a) Experimental protocol was performed on a gloved box. (b) Successful suture tied on gloved box.

ond between the two sites, allowing the network architecture to remain unmodified. HaiVision Inc. (Montreal, Canada) provided a hardware codec that used MPEG-2 and transmitted the video signal at 800 kbps.

Two surgeons, Dr Timothy Broderick and Dr Lynn Huffman from the University of Cincinnati, performed a set of tasks including touching a series of landmarks and suturing on a gloved box. The gloved box was marked with a circle and a grid of landmarks spaced 1 cm apart left to right and 0.5 cm apart toward and away as shown in Figure 10(a). The landmarks were put in a numeric sequence starting with 1 at the upper left, 2 upper right, moving down through the rows, finishing at the lower right. The following five tasks were part of the experimental protocol.

1. Right tool touches each landmark in numeric order.
2. Left tool touches each landmark in numeric order.
3. Touch each landmark in numeric order using alternating left and right tool. Right tool touches the odd numbered landmarks (left column), left tool touches the even numbered ones (right column).
4. Right tool traces inner edge of circle in a clockwise direction.
5. Left tool traces inner edge of circle in a clockwise direction.

During three days of field deployment, kinematic data of the surgeons' commands and the surgical manipulators' motions were collected along with network characterization data. Figure 11 shows the tool tip path of Dr Broderick touching each of the dots with his left hand. Deploying the system into a field environment and successfully executing the experimental protocol demonstrated the feasibility of performing mobile robotic telesurgery through a wireless communication link with limited bandwidth and variable time delays in an extreme or remote environment.

5.2. Imperial College, London, England, to University of Washington, Seattle, WA, USA.

In collaboration with Julian Leung, George Mylonas, Sir Ara Darzi, and Ghuang Zhong Yang from Imperial College (London, England) we demonstrated the ability of the RAVEN to operate across a long distance. On July 20, 2006, in the lab in Imperial College London (ICL), the surgeon site was set up with two PHANToM 6-DOF Premium haptic devices and our surgeon console software. iChat (Apple Computer Inc) was used for video feedback. The patient site was run from our lab in Seattle, WA. Time delay between the patient and surgeon sites was about 140 ms for Internet latency (measured by ping) and about 1 second for video encoding/decoding. This experiment showed that the master console software was general enough to adapt to other PHANToM devices, and also demonstrated the system's ability to teleoperate over long distances. During this experiment, the remote surgeons performed the same set of tasks on the gloved box as were performed during HAPs/MRT. Figure 13 shows the tool path of Dr Leung tracing out the circle.

5.3. Animal Lab

On March 8, 2007, in collaboration with the University of Washington Center for Video Endoscopic Surgery (UW CVES), three surgeons performed surgical tasks on a live porcine model (UW-IACUC approval #2469-04, "Robotic Surgery"). The tasks involved measuring out a specified length of bowel as well tying a suture. The patient site was set up in the animal lab, with the surgeon site in an adjacent office. Video feedback was sent directly through an S-video cable that ran between the two rooms. Figure 14 shows the surgeon in

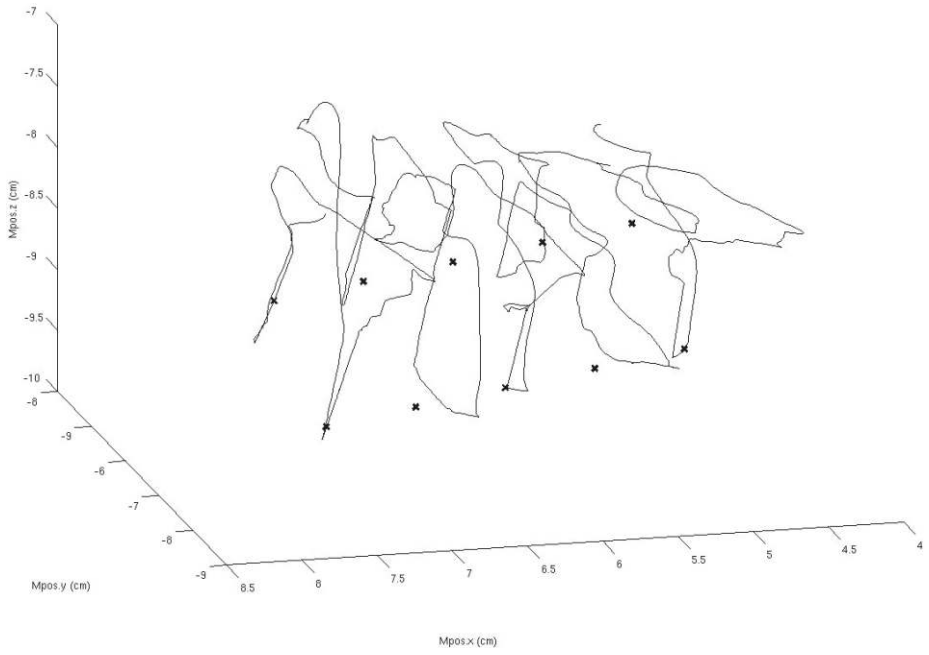

Fig. 11. Tool tip trajectory for Task 2 (touch each dot with the left hand) while operating through UAV. The crosses represent the location of each dot.

Fig. 12. Surgical robot system deployed in a remote field in Simi Valley, CA.

one room tying a suture on a piece of bowel, with the patient in the next room. This experiment was a step towards proving that the RAVEN could operate on a real patient, not just on dry-lab task boards.

5.4. NASA Extreme Environment Mission Operations (NEEMO) XII

5.4.1. TeleRobotic FLS

In the area of surgical robotics there is no clinically relevant testing standard. As we did in HAPs/MRT and with our ICL collaborations, each set of researchers devises their own experimental protocol by which to test their system. The same was true in surgery until the late 1990s when SAGES created a committee to develop a curriculum for teaching the FLS. The outcome is a curriculum that includes both cognitive and psychomotor skills. The FLS skills tasks have been validated to show significant correlation between score and postgraduate year (Derossis et al. 1998). These tasks have been used to quantitatively assess the skill of thousands of surgeons ranging from novice to expert and are considered by many the "gold standard" in surgical skill assessment.

To move toward a standard for surgical robot evaluation and testing, we have adopted the FLS skills tasks to use in our experiments. The NASA NEEMO XII mission was our first use of the new task set, with the FLS peg board transfer (also known as a block transfer) task, shown in Figure 15, chosen as the primary skills task. In the SAGES implementation of this task, the surgeon uses MIS graspers to move all six blocks from one side to the other, then back. The order does not matter, but blocks picked up on the left must be picked up with the left tool, transferred in the air to the right tool, and then set down on any peg on the right (and vice versa). The score is a proprietary formula based on completion time for the task as well as the number of errors (errors defined as a block dropped outside the black boundaries (shown in Figure 15)). The TeleRobotic FLS block transfer in contrast is more structured. The pegs are numbered and blocks must be transferred in order from left to right then right to left. The time to transfer each

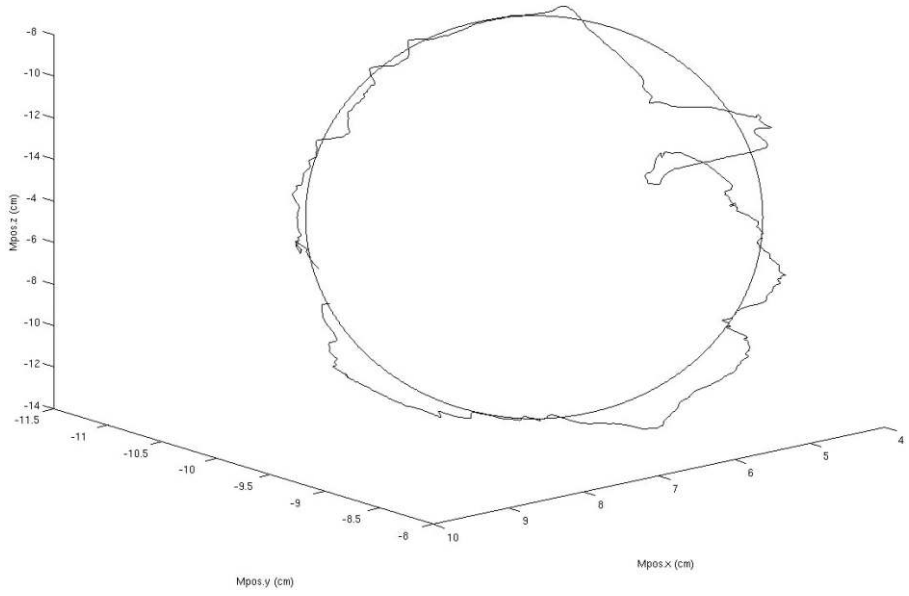

Fig. 13. Tool tip trajectory for Task 4 (trace the circle with right hand) while operating between Seattle, WA and London, England.

block is recorded for a total of 12 block transfer times per trial. Errors are classified as either Type 1 (dropped and recovered) or Type 2 (dropped and not recovered). The data reported are the mean block transfer time as well as the number of each type of error.

5.4.2. NEEMO Experiments

On May 7, 2007 the RAVEN began its 3-day deployment as part of the large-scale 12-day training exercise. The NEEMO missions are training analogs to space flight that train not only astronauts but also support personnel on how to run missions. These missions take place in the Florida Keys at the National Undersea Research Center (NURC) in Key Largo, FL and at the Aquarius Undersea Habitat, 3.5 miles offshore at a depth of 60 ft.

During our experiment, the surgeon site was set up in a conference room in Seattle, WA. The patient site was set up and supported by two surgeons inside Aquarius. Communication between the patient and surgeon sites travelled between UW and NURC via commercial Internet, then from NURC across a wireless microwave communication link to the life support buoy, and down a hardwired umbilical into Aquarius.

In order to gather network performance characteristics, a UDP packet reflector program was placed at the servers at NURC and Aquarius in Florida. The UDP packet reflector program receives the UDP data packets and routes them to back to the sender, in this case, back to our workstation at the UW. A similar UDP data structure used in the telesurgery experiments were used for the performance measurements. Each UDP data packet was time stamped at the workstation in UW and sent to the servers at NURC and Aquarius and the reflected packets were used to measure the elapsed round-trip time between the two locations. UDP packet sequence number was also used to measure the number of lost and out-of-sequence packets during the tests.

6. Results

The RAVEN was conceived from a close collaboration between engineers and surgeons. The system is a new platform for telesurgery experiments. Table 2 summarizes the mean network latency during five different experiments. The total delay experienced by the surgeon during teleoperation is a function of both network latency as well as video compression and decompression times. Depending on the video codec used video latency can vary dramatically and is difficult to measure accurately. During these telesurgery experiments, data to characterize the network conditions was collected. Figure 16 shows a histogram of the network conditions during NEEMO.

The SAGES FLS skills tasks are well defined and the kit readily available for purchase. Developing a “TeleRobotic FLS” protocol will give consistency to telesurgical experiments. Figure 17 summarizes the mean completion time for expert surgeon E1 performing the block transfer task. In each of the first three weeks of training, E1 performed three repetitions of the block transfer in the lab environment with effectively no delay. There is a learning effect as E1’s mean time improved from week to week. During the NEEMO mission,

Table 2. Summary of Experiments, Mean Network Latency and Significance of Each

Experiment	Mean Network Latency (ms)	Significance
HAPs/MRT	16	Operated in a field environment to test ruggedness and portability. Communicated via wireless through a UAV.
ICL	172	Adaptability of surgeon site to other Sensable devices. Teleoperation over long distance.
Animal lab	1	Demonstrated ability to operate on a real patient through MIS ports.
NEEMO Aquarius	76	TeleRobotic FLS for performance measurement. Operating in a unique environment. Communicating across both commercial Internet and long-distance wireless.
NEEMO NURC	75	Additional opportunity to collect TeleRobotic FLS data over long communication network.

(a)

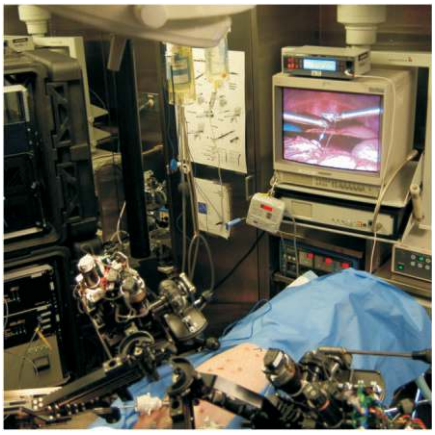

(b)

Fig. 14. (a) The surgeon controls (b) RAVEN and successfully ties a knot.

there was limited time, so E1 was only able to complete a single repetition with the RAVEN in Aquarius and another single repetition with it on-shore in Key Largo. While these results

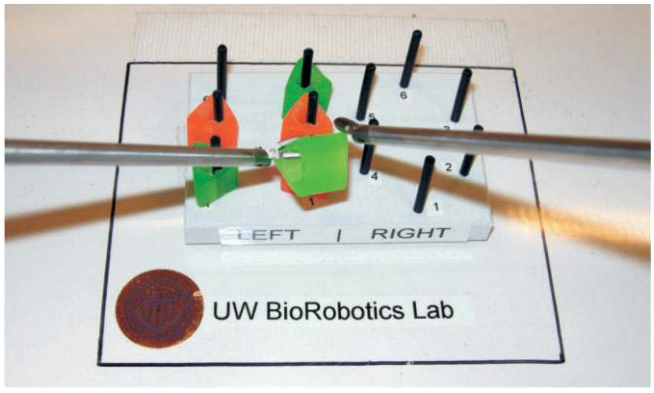

Fig. 15. The SAGES FLS block transfer task board setup with the RAVEN moving a block from left to right.

do not show statistical significance, one can observe a learning effect most likely due to accommodating for telesurgery latency. In comparison, the same surgeon, who uses a da Vinci clinically, was able to complete the block transfer task in about one minute using the da Vinci, taking only slightly longer with the stereo capability disabled. The da Vinci results are also included in Figure 17.

7. Conclusions

Starting with an extensive database of *in-vivo* minimally invasive surgical measurements, the requirements for tissue manipulation and tool handling were defined. Using a clinically relevant design specification, a kinematic optimization was performed on a spherical mechanism to obtain the ideal link lengths for the surgical manipulator. The mechanical design of the manipulators minimizes inertia through careful design of the link structure and placement of all of the actuators on a stationary base. RTAI-based control software was developed in conjunction with a USB-interface board allowing for

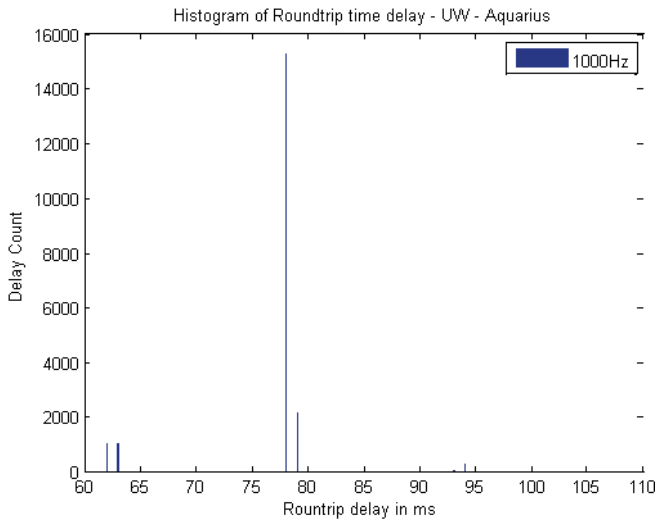

Fig. 16. Histogram of packets with respect to delay between (a) UW and Aquarius and (b) UW and NURC.

high-performance real-time control of the system. Integrating commercially available haptic devices into the surgeon console provided an inexpensive solution to surgeon site control of the surgical manipulators and enabled many collaboration opportunities. We have created a platform upon which further telesurgery experiments will be based.

8. Future Development

8.1. TeleRobotic FLS

Successful completion of multiple teleoperation experiments has demonstrated the system's ability to perform both within

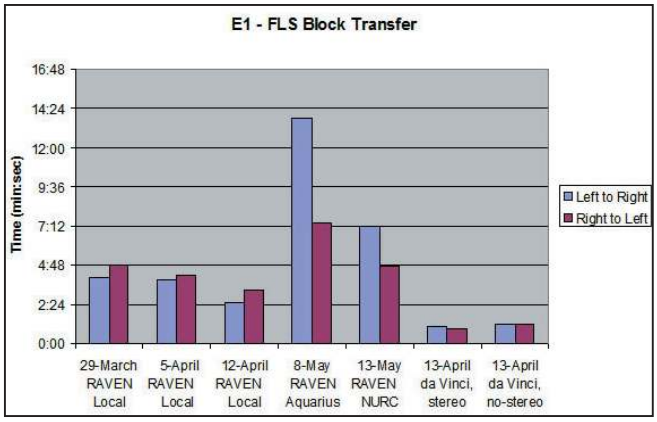

Fig. 17. Average block transfer completion times of surgeon E1 during local training on the RAVEN as well as during the NEEMO mission. Completion times using an ISI da Vinci are included for comparison.

our own lab as well as in extreme environments. In these teleoperation experiments, time delay was a challenge for the remote surgeon to overcome. From our initial experiments it is clear there is a distinct learning effect when performing a relatively simple task with the RAVEN. A training protocol has been developed to study learning on the RAVEN. Further studies will investigate surgeons performing SAGES FLS tasks under a variety of emulated time delay and network conditions. Knowledge of how surgeons adapt and perform under time delay will have a great impact on the future of telesurgery.

8.2. Bilateral Teleoperation

One of the many goals of robotic surgery is to provide the surgeon with an augmented sense of touch. Bilateral teleoperation, or force feedback, is a challenging problem. A large obstacle that has been the subject of separate research is force feedback teleoperation across long distances with time delay. The RAVEN currently does not have direct force or position sensing at the tool tip. Position measurement is taken at the actuator with the tool tip position inferred from the kinematics of the system, but this measurement does not take into account the compliance of the cable actuation system or the flexibility of the long and slender MIS tools. Force/torque sensors that are small enough to pass through the MIS port and are sterilizable would be a vast improvement to the sensing problem.

Acknowledgments

Development of the RAVEN was supported by the US Army, Medical Research and Materiel Command, grant number

DAMD17-1-0202. The HAPs/MRT project was supported by the US Army, Medical Research and Materiel Command grant number W81XWH-05-2-0080. The authors would like to thank our HAPs/MRT collaborators at the University of Cincinnati, AeroVironment, and HaiVision as well as our collaborators in London at Imperial College. The NEEMO XII participation has been supported by the US Army TATRC grant number W81XWH-07-2-0039. The authors would like to thank our NEEMO collaborators from University of North Carolina at Wilmington, US Navy, National Undersea Research Center, National Oceanographic and Atmospheric Administration, NASA, and the University of Cincinnati.

References

Berkelman, P., Boidard, E., Cinquin, P. and Troccaz, J. (2003). LER: The Light Endoscope Robot. *IEEE/RSJ International Conference on Intelligent Robots and Systems*, vol. 3, pp. 2835–2840.

Cavusoglu, M., Williams, W., Tendick, F. and Sastry, S. (2003). Robotics for telesurgery: second generation Berkeley/UCSF laparoscopic telesurgical workstation and looking towards the future applications. *Industrial Robot*, **30**(1): 22–29.

Checcacci, D., Sotgiu, E., Frisoli, A., Avizzano, C. and Bergamasco, M. (2002). Gravity compensation algorithms for parallel haptic interface. *Proceedings 11th IEEE International Workshop on Robot and Human Interactive Communication 2002*, pp. 140–145.

Cleary, K. and Nguyen, C. (2001). State of the art in surgical robotics: clinical applications and technology challenges. *Computer Aided Surgery*, **6**(6): 312–328.

Davies, B. (2000). A review of robotics in surgery. *Proceedings of the Institution of Mechanical Engineers, Part H: Journal of Engineering in Medicine*, **214**(1): 129–140.

Davies, B., Hibberd, R., Coptcoat, M. and Wickham, J. (1989). A surgeon robot prostatectomy—a laboratory evaluation. *Journal of Medical Engineering and Technology*, **13**(6): 273–277.

Derossis, A., Fried, G., Abrahamowicz, M., Sigman, H., Barkun, J. and Meakins, J. (1998). Development of a model for training and evaluation of laparoscopic skills. *American Journal of Surgery*, **175**: 482–487.

Ghodoussi, M., Butner, S. and Wang, Y. (2002). Robotic surgery—the Transatlantic case. *Proceedings IEEE International Conference on Robotics and Automation*, vol. 2, pp. 1882–1888.

Guthart, G. and Salisbury, J., J.K. (2000). The Intuitive Telesurgery System: overview and application. *Proceedings IEEE International Conference on Robotics and Automation*, vol. 1, pp. 618–621.

Harris, S., Arambula-Cosio, F., Mei, Q., Hibberd, R., Davies, B., Wickham, J., Nathan, M. and Kundu, B. (1997). The Probot—-an active robot for prostate resection. *Proceedings of the Institution of Mechanical Engineers, Part H: Journal of Engineering in Medicine*, **211**: 317–325.

Hill, J., Green, P., Jensen, J., Gorfu, Y., and Shah, A. (1994). Telepresence surgery demonstration system. *Proceedings IEEE International Conference on Robotics and Automation*, vol. 3, pp. 2302–2307.

Hongo, K., Kobayashi, S., Kakizawa, Y., Koyama, J., Goto, T., Okudera, H., Kan, K., Fujie, M., Iseki, H. and Takakura, K. (2002). NeuRobot: telecontrolled micromanipulator system for minimally invasive microneurosurgery—preliminary results. *Neurosurgery*, **51**(4): 985–988.

Jacobs, L. (1997). Determination of the learning curve of the AESOP robot. *Surgical Endoscopy*, **11**(1): 54–55.

Kobayashi, E., Masamune, K., Sakuma, I., Dohi, T. and Hashimoto, D. (1999). A new safe laparoscopic manipulator system with a five-bar linkage mechanism and an optical zoom. *Computer Aided Surgery*, **4**(4): 182–192.

Kwoh, Y., Hou, J., Jonckheere, E. and Hayati, S. (1988). A robot with improved absolute positioning accuracy for CT guided stereotactic brain surgery. *IEEE Transactions on Biomedical Engineering*, **35**(2): 153–160.

Lavallèe, S., Troccaz, J., Gaborit, L., Cinquin, P., Benabid, A. and Hoffmann, D. (1992). Image guided operating robot: a clinical application in stereotactic neurosurgery. *Proceedings IEEE International Conference on Robotics and Automation*, vol. 1, pp. 618–624.

Lum, M. (2004). Kinematic optimization of a 2-DOF spherical mechanism for a minimally invasive surgical robot. *Master's Thesis*, University of Washington.

Lum, M., Rosen, J., Sinanan, M. and Hannaford, B. (2006). Optimization of a spherical mechanism for a minimally invasive surgical robot: theoretical and experimental approaches. *IEEE Transactions on Biomedical Engineering*, **53**(7): 1440–1445.

Madhani, A., Niemeyer, G. and Salisbury, J. (1998). The Black Falcon: a teleoperated surgical instrument for minimally invasive surgery. *Proceedings IEEE/RSJ International Conference on Intelligent Robots and Systems*, vol. 2, pp. 936–944.

Marescaux, J., Leroy, J., Gagner, M., Rubino, F., Mutter, D., Vix, M., Butner, S. and Smith, M. (2001). Transatlantic robot-assisted telesurgery. *Nature*, **413**: 379–80.

Mitsuishi, M., Arata, J., Tanaka, K., Miyamoto, M., Yoshidome, T., Iwata, S., Hashizume, M. and Warisawa, S. (2003). Development of a remote minimally-invasive surgical system with operational environment transmission capability. *Proceedings IEEE International Conference on Robotics and Automation*, vol. 2, pp. 2663–2670.

Robinson, T. and Stiegmann, G. (2004). Minimally invasive surgery. *Endoscopy*, **36**(1): 48–51.

Rosen, J., Brown, J., Chang, L., Sinanan, M. and Hannaford, B. (2006). Generalized approach for modeling minimally invasive surgery as a stochastic process using a discrete

Markov model. *IEEE Transactions on Biomedical Engineering*, **53**(3): 399–413.

Rovetta, A., Sala, R., Wen, X. and Togno, A. (1996). Remote control in telerobotic surgery. *IEEE Transactions on Systems, Man, and Cybernetics Part A: Systems and Humans*, **26**(4): 438–444.

Sackier, J., Wooters, C., Jacobs, L., Halverson, A., Uecker, D. and Wang, Y. (1997). Voice activation of a surgical robotic assistant. *The American Journal of Surgery*, **174**(4): 406–409.

Sim, H., Yip, S. and Cheng, C. (2006). Equipment and technology in surgical robotics. *World Journal of Urology*, **24**(2): 128–135.

Taylor, R., Funda, J., Eldridge, B., Gomory, S., Gruben, K., LaRose, D., Talamini, M., Kavoussi, L. and Anderson, J. (1995). A telerobotic assistant for laparoscopic surgery. *IEEE Engineering in Medicine and Biology Magazine*, **14**(3): 279–288.

Taylor, R., Mittelstadt, B., Paul, H., Hanson, W., Kazanzides, P., Zuhars, J., Williamson, B., Musits, B., Glassman, E. and Bargar, W. (1994). An image-directed robotic system for precise orthopaedic surgery. *IEEE Transactions on Robotics and Automation*, **10**(3): 261–275.

Taylor, R., Paul, H., Mittelstadt, B., Glassman, E., Musits, B. and Bargar, W. (1989). Robotic total hip replacement surgery in dogs. *Proceedings of the International Conference of the IEEE Engineering in Engineering in Medicine and Biology Society*, vol. 3, pp. 887–889.

Zemiti, N., Morel, G., Ortmaier, T. and Bonnet, N. (2007). Mechatronic design of a new robot for force control in minimally invasive surgery. *IEEE/ASME Transactions on Mechatronics*, **12**(2): 143–153.